Eur. Phys. J. A **13**, 93–98 (2002)

THE EUROPEAN PHYSICAL JOURNAL A

Shell effects and pairing correlations in fission investigated with radioactive beams

J. Benlliure[1], A.R. Junghans[2], and K.-H. Schmidt[3]

[1] Universidad de Santiago de Compostela, 15706 Santiago de Compostela, Spain
[2] University of Washington, Center for Experimental Nuclear Physics and Astrophysics, BOX 354290, Seattle WA 98195, USA
[3] Gesellschaft für Schwerionenforschung, Planckstrasse 1, 64291 Darmstadt, Germany

Received: 1 May 2001 / Revised version: 13 July 2001

Abstract. The secondary-beam facility at GSI allows to produce a large variety of exotic nuclei at relativistic energies. This technique offers a unique oportunity to investigate systematically fission in inverse kinematics. In the present experiment, the fission properties of more than 70 different actinides and preactinides were investigated at low excitation energy. The elemental yields and kinetic energies of the fission residues present new signatures of shell structure and pairing correlations.

PACS. 24.75.+i General properties of fission – 25.85.-w Fission reactions – 25.70.Mn Projectile and target fragmentation – 25.60.-t Reactions induced by unstable nuclei

1 Introduction

Nuclear fission constitutes the most clear example of a large-scale collective motion of nuclear matter governed by the interplay between nuclear dynamics and shell structure. The characterization of this process at low excitation energy is expected to provide information about shell structure at large deformation and the viscosity of cold nuclear matter.

It is well known that the different fission modes observed in the mass and charge distributions of fission residues are a manifestation of shell structure [1,2]. Previous existing results [3] indicate an evolution of the fission modes according to the mass number of the fissioning nucleus. Nuclei with masses between 230 and 256 present a double-humped mass distribution which is explained by the shell closure around the spherical shell $N = 82$ and the deformed one at $N \approx 90$. In contrast, heavier or lighter nuclei have single-humped distributions.

Pairing correlations have also been observed in even fissioning nuclei at low energy as an enhanced production of fission residues with even proton or neutron number. This observation was interpreted as the survival probability of the superfluid phase of cold nuclear matter in the path from saddle to scission determined by the nuclear viscosity [4]. The evolution of the even-odd effect for different fissioning nuclei was explained in terms of the different saddle-scission configurations while the evolution for different mass or charge splits of the same system was concluded to be originated by different temperatures in the fission modes [5].

Unfortunately, the experimental information about fission is rather restricted, and our present knowledge on fission could suffer from this limitation. Only few nuclei have been intensively investigated because of their applications. The main reason for this lack of experimental information on fission is that nature provides only four fissile stable nuclides and only few more long-lived ones decay spontaneously by fission. In addition, standard fission reactions can only be studied with stable or long-lived target nuclei.

Relativistic radioactive beams offer a new access to fission that overcomes the previous limitations. In this work, we review the main results obtained in the first experiment performed at GSI where the fission of relativistic secondary beams was investigated in flight. In this experiment the charge and kinetic-energy distributions of the fission residues were used to obtain information about the role of shell structure and pairing correlations in fission.

2 The experiment

The secondary-beam facility at GSI was used to produce more than 70 different neutron-deficient actinides and preactinides by fragmentation of a ^{238}U beam at 1 A GeV in a 657 g/cm^2 Be target. The fragmentation residues were separated and identified using the fragment separator FRS [6]. The acceptance of the separator allowed to produce multi-isotopic secondary beams and consequently to investigate simultaneously the fission properties of more than 20 different nuclides [7]. References [8,9] provide a detailed description of the technique used to produce the secondary beams. These secondary beams were guided to a

specific experimental set-up to investigate fission induced in a second target. The whole experiment is described in detail in ref. [10].

The main limitation of any experiment with secondary beams is the primary-beam intensity since two consecutive reactions are involved. In that sense many of the parameters of the experiment should be optimized. Reaction cross-sections and target thicknesses play a major role but also the acceptance of the experimental set-up and the kinematical conditions do. In our case, the relativistic energy of the secondary beam is one of the key parameters. At these energies, the separation of the secondary beam is optimum, and the target thicknesses can be larger. In addition, we have a high transport efficiency of the secondary beam and the reaction residues are forwardly focussed, simplifying the detection set-up.

2.1 Experimental technique for fission studies

In order to investigate the role of shell structure and pairing correlations at low energy, fission was induced by Coulomb excitation of the secondary beam in the electromagnetic field of a high-Z target nucleus. The main advantages of this reaction mechanism is that its cross-section is relatively high and the excitation energy range is around the fission barrier. In addition, a dedicated set-up was used to measure the nuclear charge and kinetic energy distributions of the fission residues.

To suppress fission events produced in other layers of matter and to improve the resolution in kinetic energy, an active secondary target made of 5 foils of lead was used. The total thickness of the target was 5 g/cm^2. The charge and the kinetic energy of the fission residues were determined from the measurement of their energy loss and time of flight. The energy loss was measured in a vertically subdivided multi-sampling ionisation chamber (twin MUSIC) with a common cathode and four anodes in the upper and lower chambers. In addition, it provided the tracking of both fission residues. The vertical position was determined by the drift time while the horizontal one was given by the pulse-height ratio of the signals recorded by the diagonally subdivided anodes.

The velocities of both fission residues were provided by the time-of-flight measurement between a plastic scintillator placed in front of the active target and a plastic-scintillator wall located 5 meters behind. This measurement was used to correct the velocity dependence of the energy loss measured with the MUSIC and to determine the kinetic energy of the fission residues. All the detectors were designed in order to accept all the fission fragments produced in the active target. The detector efficiency amounted to 81%.

After separation, the average energy of the secondary beam was around 500 A MeV. At this energy, the equivalent photon spectrum produced by a lead target is hard enough to excite the giant resonances of the secondary projectiles. Although the present set-up did not allow to determine the excitation energy of the fissioning nucleus, the excitation energy distribution could be calculated on the basis of theoretical considerations as described in ref. [10]. According to this calculation, the excitation energy spectra of all the investigated nuclei are very similar. They peak at 11 MeV with a tail to higher energies, corresponding to the decreasing intensity of the equivalent photon spectrum.

2.2 Data evaluation

The fission-fragment element distributions were obtained from the energy loss signals measured in the twin ionisation chamber corrected by their velocity determined with the time of flight. The main difficulty of the data evaluation was the distinction between electromagnetic- and nuclear-induced fission. For this purpose, the fission fragments produced in the active target and in the first plastic scintillator were registered. Different conditions were used to distinguish between these two reaction mechanisms.

Fission induced in other layers of matter was disregarded by the analysis of the energy loss signals in the active target. In addition, a first selection of electromagnetic-induced fission was done by imposing the condition that the charge sum of the fission fragments equals the nuclear charge of the secondary projectiles. Proton evaporation after electromagnetic excitation is very unlikely for the nuclei investigated due to the Coulomb barrier. In order to subtract the remaining contribution due to nuclear-induced events where only neutrons are removed, the fission events produced in the plastic scintillator and the active target were compared. Fission events in the plastic scintillator are expected to be produced only by nuclear interaction, and their appropriately weighted nuclear-charge spectrum was subtracted from the one obtained in the active target.

The total kinetic energy of the fission fragments was deduced from their velocity vectors, transformed into the center-of-mass frame of the fissioning secondary projectile. The details of this procedure are described in refs. [10,11]

3 Results

In the present experiment, the elemental yields and the total kinetic energies of fission residues produced by Coulomb excitation of long isotopic chains of secondary projectiles from ^{205}At to ^{234}U have been determined. In fig. 1, we report in a chart of the nuclides the elemental distributions of fission residues in the range $Z = 24$ to $Z = 65$ after fission of 28 secondary beams between ^{221}Ac and ^{234}U. The whole experimental information obtained in this experiment can be found in ref. [10].

These data allow for the first time to systematically analyze the fission properties of nuclei in a continuously covered region of the chart of the nuclides. Two main features can be observed in the elemental charge distributions: a coarse structure which corresponds to the fission modes and a fine odd-even effect.

Figure 1 shows that the transition from symmetric fission in the lighter elements to asymmetric fission in the

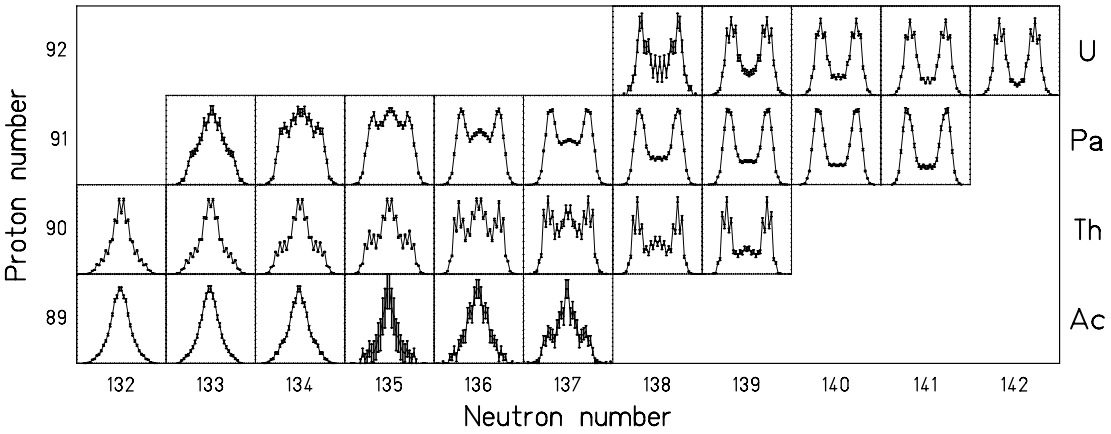

Fig. 1. Measured fission-fragment nuclear-charge distributions in the range $Z = 24$ to $Z = 65$ after electromagnetic excitation of 28 secondary projectiles in a lead target between ^{221}Ac and ^{234}U shown in a chart of the nuclides.

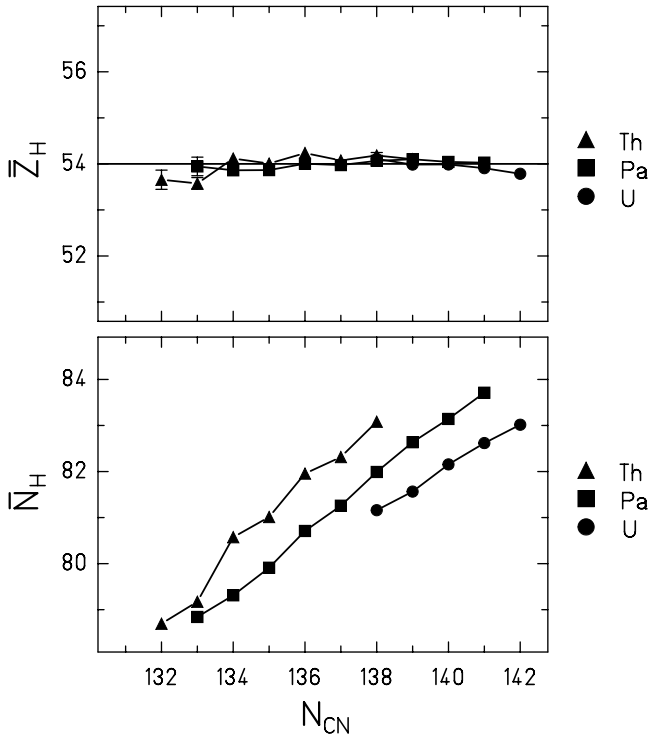

Fig. 2. Mean position of the heavy-asymmetric component of the fission-fragment distributions in nuclear charge (upper part) and neutron number (lower part) as a function of the neutron number of the fissioning secondary projectile. While the charge number was measured, the neutron number was estimated by the UCD assumption.

heavier ones is systematically covered by the present data. In the transitional region, around ^{226}Th, triple-humped distributions appear with comparable intensities for symmetric and asymmetric fission. A clear even-odd effect is observed for the even fissioning elements U and Th.

3.1 Shell effects in fission

According to the present understanding of the fission process, the asymmetric components appearing in the element distribution of the fission residues are attributed to valleys in the potential-energy surface seen by the fissioning system in the path from saddle to scission due to shell effects. These shells determine the positions and the yields of the components observed in the element distributions of the fission residues.

In order to determine the positions of the fission components we fitted three Gaussians to the measured nuclear-charge distributions. In the upper part of fig. 2 we report the mean position of the heavy asymmetric component of the measured fission-fragment element distributions as a function of the neutron number of fissioning secondary projectiles of three elements uranium, protactinium and thorium. The equivalent position in neutron number was deduced using the UCD (unchanged charge density) assumption, and the results are reported in the lower part of fig. 2. This analysis shows clearly that the position of the heavy component is almost constant around the atomic number $Z \approx 54$ while it moves considerably in neutron number. This means that the position in mass number also moves.

This is a surprising result since, according to previously measured fission-fragments mass distributions, the position of the heavy fission component was found to be almost constant in mass number [3]. This observation had been explained as a consequence of the strong influence of the neutron shell in the heavy component [12]. The analysis of the new data, which allow for the first time to follow the element distributions over long isotopic sequences of the fissioning system, seems to indicate that the role of shell effects in proton number play a more important role in fission than previously thought.

The interpretation of the observed evolution of the fission components would require a full theoretical description of the fission process. A realistic model should include not only a description of the potential-energy surface but also the dynamics of the collective motion from saddle to scission. Some recent work concentrates on the description of the potential-energy surface including structure effects [13,14]. Very recently, two-dimensional fission-fragment mass-energy distributions were obtained from

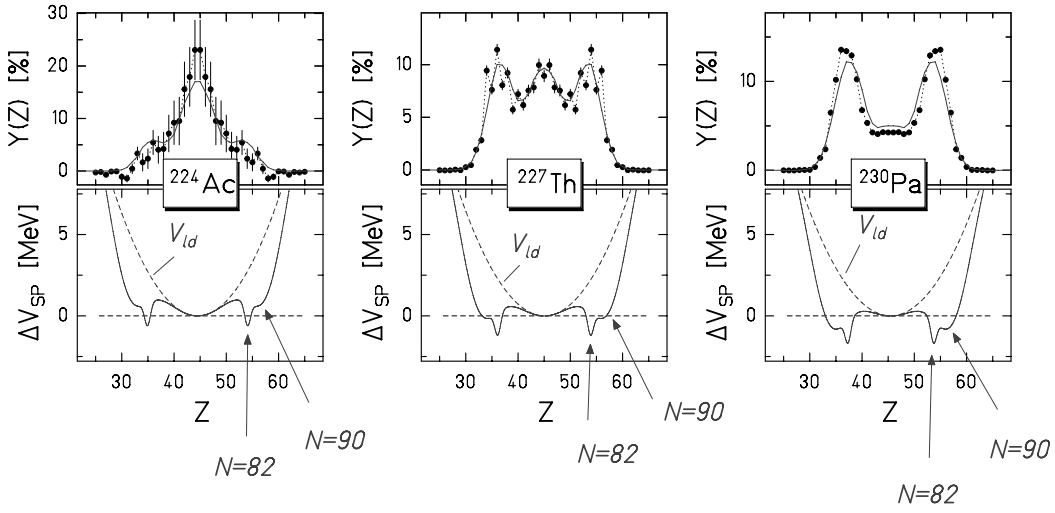

Fig. 3. Measured element yields compared to the model predictions (upper part), and description of the mass-asymmetric potential energy above the macroscopic barrier used to calculate the statistical weight of transition states for each splitting (lower part).

most advanced multi-dimensional Langevin calculations (*e.g.*, [15]) on the basis of the liquid-drop model with a finite range of the nuclear forces and a modified one-body mechanism for nuclear dissipation. However, to our knowledge, a complete dynamical description of low-energy fission which includes the influence of shell effects and pairing correlations is not yet available.

Since theory cannot yet provide a full realistic description of the process, we tried to understand the data with a semi-empirical approach. In our description the population of the fission channels is assumed to be basically determined by the statistical weight of transition states above the potential-energy landscape near the fission barrier. Several properties, however, are finally determined at scission. A full description of the model is given in ref. [16].

The barrier as a function of mass asymmetry is defined by three components. The first is the symmetric component $V_{\rm ld}$ defined by the liquid-drop potential by means of a parabolic function with a curvature obtained from experimental data [17]. This parabola is assumed to be modulated by two neutron shells, located at mass asymmetries corresponding to the neutron numbers $N = 82$ (spherical neutron shell) and $N \approx 90$ (deformed neutron shell). We assume that the mass-asymmetric degree of freedom at the fission barrier is on average uniquely related to the neutron number of the fragments. The shells are represented by Gaussian functions. The population of the fission channels is proportional to the level density around the corresponding dips in potential at a given excitation energy. Shells are supposed to wash out with excitation energy [18]. The heights of these Gaussians are the only parameters in the model which were adjusted to describe the measured yields for ^{227}Th. Other parameters, like the widths of these Gaussians and additional fluctuations in mass asymmetry adquired from saddle to scission are derived from idependent data [16].

The lower pictures in fig. 3 represent the mass asymmetric potential for three different fissioning nuclei: ^{224}Ac, ^{227}Th and ^{230}Pa. In these pictures the dashed lines represent the macroscopic liquid-drop component of the potential and the solid lines the full potential including the shell correction. The shell effects in neutron number are the same for the three systems. Fluctutations in the neutron-to-proton ratio are also considered by describing the potential in this degree of freedom by a parabolic function. Asumming that the equilibration in this variable is fast compared to the saddle-to-scission time, the curvature of this potential was calculated in a touching-sphere configuration.

In the upper part of fig. 3 we compare some measured element yields with the model predictions using realistic estimates [19] of the excitation-energy distribution acquired by electromagnetic excitation. As can be seen, the evolution of the stiffness of the macroscopic liquid-drop potential explains the evolution from asymmetric to symmetric fission. The good description of these three systems is valid for any of the measured charge distributions as shown in ref. [19], although the position of the asymmetric component varies slightly around $Z = 54$. From this success of the very simple model we conclude that the relative yields of the different fission components can be understood in the transition-state model by the global features of the mass-asymmetry–dependent potential at saddle due to the interplay of liquid-drop properties and the different shell effects. The next step would be to introduce the potential resulting from a full shell-model calculation which includes more shells, also in the proton number.

3.2 Pairing correlations in fission

The second structure which appears in the measured element distribution is the enhanced production of fission

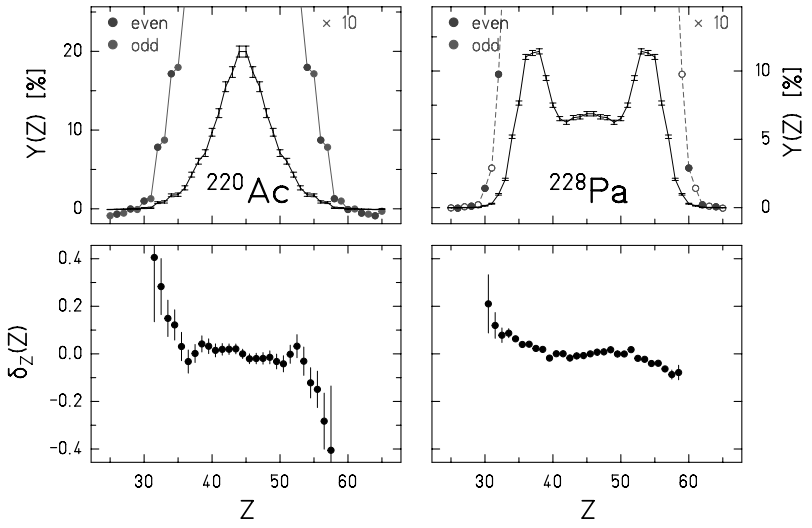

Fig. 4. Measured element distributions (upper part) and deduced local even-odd effect (lower part) after electromagnetic-induced fission of ^{220}Ac and ^{228}Pa.

residues with even proton number. While the neutron number of the fission fragments is mainly determined by the evaporation from the excited fragments, the proton number provides a direct information about the charge split at scission.

The enhanced production of fission fragments with even proton number has been interpreted as a direct measure of the quasi-particle excitation at scission [5] that would provide information about the fission dynamics. Once the excitation energy is sufficient to break a pair, it is assumed that the unpaired protons are distributed with equal probabilities to the two nascent fission fragments, and the odd-even effect vanishes.

The data recorded during this experiment allow a comprehensive survey on the odd-even structure in the proton numbers of fission fragments of a series of uranium, protactinium, thorium and actinium isotopes. In the upper part of figs. 4 and 5 we represent the measured charge distributions of two fissioning nuclei with an odd number of protons (Ac, Pa) and two others with an even number of protons (Th, U), respectively. In the lower part of both figures we quantify the local odd-even effects by the logarithmic third difference $\delta_p(Z)$, as introduced in ref. [20].

The analysis of the odd-Z fissioning systems reveals a surprising result. A clear positive odd-even effect for the light residues and a negative one for the heavy residues are observed. Absolute values of the local odd-even effect up to more than 20% are found for the more asymmetric charge splits. The behavior of the local odd-even effect is essentially the same for the two nuclei, although their charge distributions are different. Similar results are obtained for all the odd-Z systems investigated in this experiment [21].

In contrast to previous interpretations where no even-odd effect was expected in odd-Z fissioning systems [5], the present data give a clear evidence that the unpaired proton preferentially sticks to the heavy fission residue. The explanation can probably be found in the larger value of the single-particle level density in the heavy fission residue, which scales with the volume [21].

For even-Z fissioning nuclei (fig. 5) a completely different behavior of the local odd-even effect is observed. For all the investigated systems, there is a strong variation from a minimum value near symmetry to an increase of about a factor of two for the most asymmetric charge splits. As in the odd-Z fissioning systems, this result can be explained as a consequence of the larger single-particle level density of the heavier fragment. When a pair is broken, the unpaired protons prefer the heavier fission residue. Again, this result demands for a revision of previous interpretations, where the even-odd effect in extremely asymmetric fission of even-Z systems was understood as a measurement of the temperature at scission [22].

4 Conclusion and perspectives

The present experiment has demonstrated that relativistic radioactive beams offer a new access to fission. Radioactive beams allow to systematically investigate the fission properties of nuclei in a continuously covered region of the chart of the nuclides. The relativistic energies used in this experiment are a key parameter to fully separate and identify the secondary projectiles and to provide a high detection efficiency and a good charge identification of the fission residues. In addition, the Coulomb excitation is at the moment the optimum reaction mechanism to induce low-energy fission in inverse kinematics.

The quality of the elemental distributions of fission residues have provided new evidences of the role of nuclear structure in low-energy fission. The analysis of the asymmetric component in the charge distributions of fission residues reveals an unexpected influence of proton shells. The evolution of the fission components has been explained on the basis of a statistical population of transition states above a simple mass-asymmetric potential

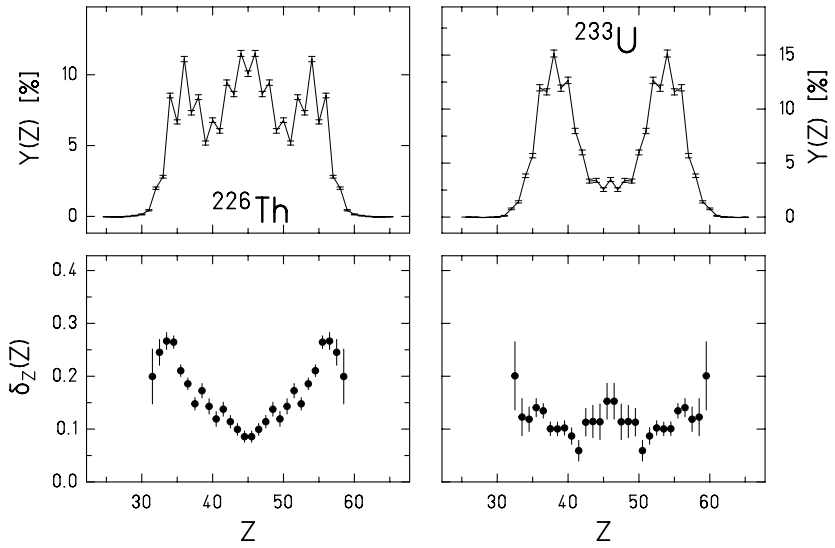

Fig. 5. Measured element distributions (upper part) and deduced local even-odd effect (lower part) after electromagnetic-induced fission of ^{226}Th and ^{233}U.

landscape determined semi-empirically. This result would indicate that the dynamics of the fission process tends to wash out the influence of the details of the potential-energy landscape.

New findings were also obtained in the analysis of the local even-odd effect of the elemental distributions of fission residues. In odd-Z fissioning systems an even-odd effect has been found in asymmetric charge splits. In the case of even-Z fissioning systems an enhancement of the even-odd effect was observed for the most asymmetric splits. Both effects have been understood by statistical arguments. The probability for the unpaired nucleons to end up in one of the fission residues is governed by the single-particle density of the final states. Consequently, the unpaired protons preferably stick to the heavier fission residue.

Besides the scientific interest in a better understanding of the influence of nuclear structure on a large-scale collective motion of nuclear matter, the knowledge brought by these investigations is relevant for several applications. The fission process is directly involved in the production of neutron-rich secondary projectiles in next-generation secondary-beam facilities and in the proposals to incinerate nuclear waste using accelerator-driven subcritical reactors.

In spite of the success of the present experiment, some improvements could be considered in the future. Concerning the experimental set-up, the most important improvement would be to perform a kinematically more complete measurement of the reaction including the mass identification of the fission residues and the multiplicity and energy of the evaporated neutrons. This measurement would require an additional magnetic dipole spectrometer and a neutron detector. This set-up would allow to investigate the influence of proton and neutron shells separately and to determine the temperature dependence of fission dynamics. Concerning the excitation mechanisms, an ambitious project would be to replace the Coulomb excitation in a lead target by inelastic electron scattering in an electron-ion collider ring.

References

1. M. Göppert-Mayer, Phys. Rev. **74**, 235 (1948).
2. L. Meitner, Nature **165**, 561 (1950).
3. K.F. Flynn *et al.*, Phys. Rev. C **5**, 1725 (1972).
4. F. Gönnenwein, *Mass, Charge and Kinetic Energy of Fission Fragments*, in *The Nuclear Fission Process*, edited by C. Wagemans (CRC Press, London, 1991) p. 409.
5. H. Nifenecker *et al.*, Z. Phys. A **308**, 39 (1982).
6. H. Geissel *et al.*, Nucl. Instrum. Methods B **70**, 286 (1992).
7. K.-H. Schmidt *et al.*, Phys. Lett. B **325**, 313 (1994).
8. M. de Jong *et al.*, Nucl. Phys. A **628**, 479 (1998).
9. A.R. Junghans *et al.*, Nucl. Phys. A **629**, 635 (1998).
10. K.-H. Schmidt *et al.*, Nucl. Phys. A **665**, 221 (2000).
11. C. Böckstiegel *et al.*, Phys. Lett. B **398**, 259 (1997).
12. B.D. Wilkins *et al.*, Phys. Rev. C **14**, 1832 (1976).
13. V.V. Pashkievich, Nucl. Phys. A **14**, 1 (1976).
14. P. Möller *et al.*, Phys. Rev. C **61**, 047602 (2000).
15. A.V. Karpov *et al.*, Phys. Rev. C **63**, 054610 (2001).
16. J. Benlliure *et al.*, Nucl. Phys. A **628**, 458 (1998).
17. S.I. Mulgin *et al.*, Nucl. Phys. A **640**, 375 (1998).
18. A.V. Ignatyuk *et al.*, Sov. J. Nucl. Phys. **29**, 450 (1979).
19. K.-H. Schmidt *et al.*, Nucl. Phys. A **685**, 60 (2001).
20. B.L. Tracy *et al.*, Phys. Rev. C **5**, 222 (1972).
21. S. Steinhäuser *et al.*, Nucl. Phys. A **634**, 89 (1998).
22. J.L. Sida *et al.*, Nucl. Phys. A **502**, 233c (1989).